Energy & Environmental Science

COMMUNICATION

View Article Online
View Journal | View Issue

Cite this: *Energy Environ. Sci.*, 2018, **11**, 551

Received 12th January 2018,
Accepted 8th February 2018

DOI: 10.1039/c8ee00122g

rsc.li/ees

Beyond catalysis and membranes: visualizing and solving the challenge of electrode water accumulation and flooding in AEMFCs†

Travis J. Omasta,[ab] Andrew M. Park,[c] Jacob M. LaManna,[d] Yufeng Zhang,[b] Xiong Peng,[ab] Lianqin Wang,[e] David L. Jacobson,[d] John R. Varcoe,[e] Daniel S. Hussey,[d] Bryan S. Pivovar[c] and William E. Mustain*[ab]

A majority of anion exchange membrane fuel cells (AEMFCs) reported in the literature have been unable to achieve high current or power. A recently proposed theory is that the achievable current is largely limited by poorly balanced water during cell operation. In this work, we present convincing experimental results – coupling *operando* electrochemical measurements and neutron imaging – supporting this theory and allowing the amount and distribution of water, and its impact on AEMFC performance, to be quantified for the first time. We also create new electrode compositions by systematically manipulating the ionomer and carbon content in the anode catalyst layer, which allowed us to alleviate the mass transport behavior limitations of H_2/O_2 AEMFCs and achieve a new record-setting peak power density of 1.9 W cm^{-2} – a step-change to existing literature. Our efforts cast a new light on the design and optimization of AEMFCs – potentially changing the way that AEMFCs are constructed and operated.

Broader context

Electrochemical energy conversion devices have the potential to provide clean, sustainable energy for grid and transportation applications in the 21st century and beyond. The incumbent technology, proton exchange membrane fuel cells (PEMFCs), have inherently high materials and systems-level costs, which has led to the emergence of anion exchange membrane fuel cells (AEMFCs) with the potential to lower these costs significantly. Unfortunately, AEMFCs have mostly been limited to low achievable current – not because of catalysis or ionic conduction, but because of poorly understood and poorly controlled electrode composition and structure – which directly impacts the transport behavior of cell water and performance. This study uses direct visualization and quantification of water in operating AEMFCs to show how systematic electrode design can enable precise control of the quantity and location of water, which allowed us to achieve record-setting 1.9 W cm^{-2} AEMFC performance, comparable to state-of-the-art PEMFCs, making this an important and timely contribution to the field. In addition to the demonstrated AEMFC technology, the lessons learned in this work can also provide transformational insights to other AEM-based electrochemical devices for energy (electrolyzers, flow batteries, CO_2 capture, and electrosynthesis), water purification (electrodialysis) and healthcare (dialyzers).

Over the past decade, interest in anion exchange membrane fuel cells (AEMFCs) has grown significantly, with the number of papers in the field increasing rapidly during this time (24 papers in 2006 *vs.* 312 in 2016, Fig. S1, ESI†).[1] The primary motivating factor for this attention is cost, as it is widely accepted that alkaline pH conditions have the potential to drive down materials-level, stack-level and systems-level costs below their proton exchange membrane fuel cell (PEMFC) counterparts, which is important for adoption into commercial markets. For example, it may be possible to either eliminate or significantly reduce the amount of platinum group metals (PGM) in the catalyst layers, as well as create drastically lower cost bipolar plates. Additionally, moving to AEMFCs allows for the use of lower cost anion-exchange membranes (AEMs) and offers the potential to decrease other balance of plant costs related to humidification and air circulation systems.[2–7]

The recent, intense effort around AEMFCs has led to the development of several highly conducting, stable AEMs and anion exchange ionomers (AEIs),[8–21] high activity catalysts – still predominantly PGM-containing at the cathode and anode,[5,6,8,22–27] although there has been recent progress on PGM free catalysts[3–6,28–33] – as well as a significant increase in state-of-the-art performance.[19–22,34] At least some of this success can be attributed to the willingness of researchers to rapidly and transparently share their accomplishments in this area over

[a] *Department of Chemical Engineering, University of South Carolina, Columbia, South Carolina 29208, USA. E-mail: mustainw@mailbox.sc.edu*
[b] *Department of Chemical & Biomolecular Engineering, University of Connecticut, Storrs, Connecticut 06269, USA*
[c] *National Renewable Energy Laboratory, Golden, Colorado 80401, USA*
[d] *National Institute for Standards and Technology, Gaithersburg, Maryland, 20899, USA*
[e] *Department of Chemistry, University of Surrey, Guildford, GU2 7XH, UK*

† Electronic supplementary information (ESI) available: Fig. S1–S5, Tables S1 and S2, experimental details and additional analysis. See DOI: 10.1039/c8ee00122g

the past few years, which has seen several international workshops dedicated to AEMFCs, with events in Guildford (UK),[35] Santa Fe (USA),[36] Wuhan (China),[37] Bad Zwischenahn (Germany),[38] and Phoenix (USA),[2] to name a few. These meetings have resulted in many cross-cutting collaborations,[4,5,8] including this one. In fact, over the past two years, state-of-the-art AEMFC peak power has doubled from $\sim$0.7 W cm^{-2} to $\sim$1.4 W cm^{-2} because of the application of PtRu catalysts in the anode,[22] emergence of highly conducting radiation-modified ethylene tetrafluoroethylene (ETFE) and low density polyethylene (LDPE) AEMs,[19,20] AEI powders,[39] and optimizing the reacting gas dew points.[19–22,34] – these advances are discussed extensively and demonstrated in Fig. S2 and Table S1, in the ESI.†

However, one area in AEMFC research where there exists a significant knowledge gap, due to a lack of fundamental investigation and modeling efforts, is the influence of electrode composition and structure, and operating conditions, on the transport properties of reactants, products, ions and water, which ultimately dictate performance. Among these, water is particularly important in AEMFCs because of its severe intrinsic imbalance.[34,40–43] In a PEMFC, water is only generated at the cathode at a rate of 2 water molecules for every 4 electrons transferred. In an AEMFC, there are 4 water molecules generated at the anode in addition to 2 water molecules consumed at the cathode for every 4 electrons transferred (Fig. 1A). This creates a water differential between the cathode and anode that is three times larger in AEMFCs than in PEMFCs (6 *vs.* 2). Additionally, the ability to influence this water balance through manipulation of anode and cathode flow rates and pre-humidification levels is greatly altered. Therefore, AEMFCs represent an entirely new learning curve with respect to the treatment of water that has not been adequately investigated to date. Properly addressing the water imbalance through new operational strategies and cell architectures is critical for AEMFCs to achieve performances comparable to those of PEMFCs and enable them to compete in the marketplace.

It was recently proposed[6,34] that the achievable current density in AEMFCs is limited in most published experimental studies by poorly balanced water during cell operation. Indirect evidence has been presented showing that simultaneously decreasing the anode and cathode gas dew points reduced flooding events and increased AEMFC current and power. In this work, we couple *operando* electrochemical measurements and neutron imaging to directly show the behavior of water before, during and after AEMFC flooding events, which allow us to answer open questions about the hydration of the membrane, catalyst layers and gas diffusion layers as well as the nature of the reacting water at the cathode – none of which have been reported previously. It was also clear from the neutron imaging, which will be discussed thoroughly later, that controlling the anode and cathode dew points are not sufficient to weed out catastrophic flooding entirely and optimize performance. To do this, the electrode composition must also be considered since the amounts and ratios of carbon, AEI and catalyst in the catalyst layer, and their distribution within the electrode structure, will play a significant role in determining cell power. Through systematic design of the catalyst layer, coupled with balancing cell water, we show a pathway to increase the achievable current in an operating AEMFC by 25% (to nearly 5 A cm^{-2} at full cell discharge) and the achievable power density by 35% (to 1.9 W cm^{-2}) compared to the existing state-of-the-art (recent high performing AEMFCs are summarized in Table S2, ESI†).[34]

To achieve the existing state-of-the-art current and power, one of the most important changes was the replacement of the Pt catalyst in the anode catalyst layer with PtRu, which previously allowed the peak power to increase from 1.05 W cm^{-2} to 1.4 W cm^{-2} (at optimized anode and cathode dew points) through improved hydrogen oxidation reaction (HOR) kinetics, Fig. S2 (ESI†). However, when researchers added Ru to the catalyst, it was done by: (i) keeping Pt loading on the electrodes the same; and (ii) maintaining the total percentage of AEI in the catalyst layer.

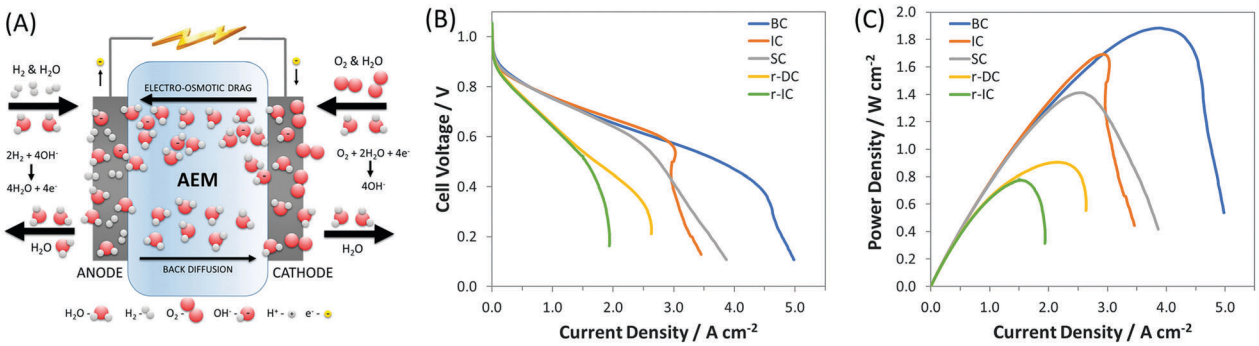

Fig. 1 (A) Schematic of AEMFC water consumption, generation, migration, and diffusion; (B) *i*–*V* and (C) *i*–power curves (10 mV s^{-1} forward scans) of AEMFCs with an ETFE-based AEM and AEI, both containing a benzyl trimethyl ammonium (BTMA) headgroup (ETFE–BTMA). The cathode for each of these were the same within experimental reproducibility, but 5 different anodes were produced (Table 1): SC – standard carbon, which is a result of how PtRu was added to the anode as a replacement for Pt; IC – increased carbon, which was done to match the AEI : C : catalyst layer while keeping the Pt : C ratio the same ratio as the best-performing Pt/C anodes; r-IC – reduced thickness (60% loading) anode with the same AEI : C : Pt ratio as the IC anode; r-DC – reduced thickness anode with the same catalyst loading as IC, but twice the carbon and ionomer; and BC – anode with a balanced AEI : C : Pt ratio. The cell temperature was fixed at 60 °C with flow rates of 1.0 L min^{-1} for H_2 and O_2 at the anode and cathode, respectively. Optimized anode/cathode dew points were applied for each test: BC (45 °C/46 °C), IC (47 °C/49 °C), SC (54 °C/57 °C), r-IC (53 °C/53 °C), r-DC (51 °C/52 °C).

Table 1 Catalyst, carbon, and ionomer loadings and ratios of all tested conditions

Anode type	SC	IC	r-IC	r-DC	BC
PtRu loading, mg cm^{-2}	0.67	0.71	0.42	0.42	0.71
Carbon loading, mg cm^{-2}	0.45	0.71	0.42	0.84	1.07
Carbon weight%	32.0%	41.4%	41.4%	52.2%	**48.0%**[a]
AEI weight%	20.0%	17.2%	17.2%	21.7%	**20.0%**[a]
AEI : C ratio	0.625	**0.417**[a]	**0.417**[a]	**0.417**[a]	**0.417**[a]
AEI : C : Pt ratio	0.625 : 1.0 : 1	0.625 : 1.5 : 1	0.625 : 1.5 : 1	1.25 : 3.0 : 1	0.94 : 2.5 : 1

[a] Optimized value.

The effect of adding Ru in this manner is that the relative amount of carbon is appreciably reduced, resulting in a thinner and less porous catalyst layer; we denote that case as SC (standard carbon) in Fig. 1 and Table 1. The thinner, less porous catalyst layer results in an anode electrode with reduced water capacity/tolerance (meaning the amount of water that can be held without flooding issues arising). The reduction in anode water capacity can limit the ability of AEMFCs to achieve, and more importantly maintain, higher current and power densities.

Therefore, the first approach to increasing the achievable current in these PtRu anode AEMFCs was to increase the pore volume and water capacity of the anode by increasing the amount of carbon in the anode. This case is denoted in Fig. 1 and Table 1 as IC (increased carbon) and was selected to achieve the same AEI : C : Pt ratio as previously reported high performing Pt/C anodes.[34] The result, shown in Fig. 1B and C, was an increase in cell power density to 1.7 W cm^{-2}, compared to SC, 1.4 W cm^{-2}, although the limiting current of IC was slightly less than SC. The limiting current behavior of the IC polarization curve showed an inflection point, Fig. 1B, which suggests that cell water management was still a concern at high current density, which can be alleviated through further electrode design and control of the AEI : C : Pt balance.

In order to better understand fuel cell *operando* water dynamics, neutron imaging experiments were done at the NIST Center for Neutron Research[44] (experimental details are provided in the ESI†), with results in Fig. 2. Cells designed for use in the neutron beam (1.2 cm^2 active area)[45] were constructed with a IC anode, Pt/C cathode (Table 1), and a radiation-grafted ETFE-based AEI powder and AEM (hydrated thickness = 50 μm).[19,39] Firstly, cell voltage was maximized at 1.5 A cm^{-2} by finding the optimal anode and cathode operating dew points −50 °C (62% relative humidity, RH) at both electrodes while ensuring stable operation (each individual cell was able to operate continuously and stably for more than 12 h). External water was then slowly added to the cell by increasing the dew points of both the anode and cathode by 1 °C (optimal +1 °C) and 2 °C (optimal +2 °C). The steady-state distribution of water at each condition with the ETFE–BTMA AEMs and ETFE–BTMA AEI-containing catalyst layers are shown as in-plane neutron radiographic images (Fig. 2A) and quantitative through-plane water distribution plots (Fig. 2B).

As the relative humidity of the gas feeds is increased, the anode experiences an increase in the amount of liquid water, with a large amount accumulating in both the anode catalyst

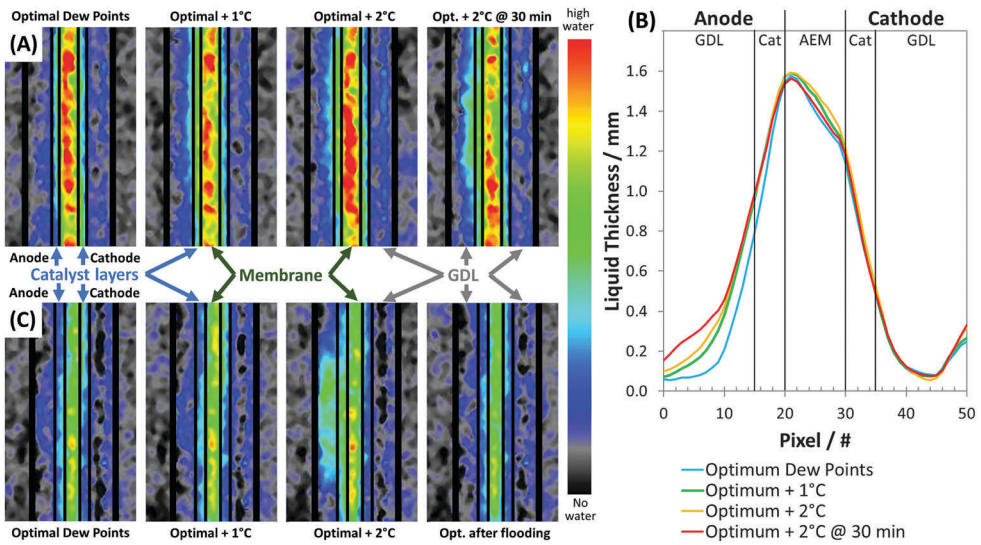

Fig. 2 (A) Operando in-plane neutron radiographic images of water in the gas diffusion layers, catalyst layers, and the radiation-grafted ETFE–BTMA AEM in an AEMFC operating at 1.5 A cm^{-2}, 60 °C, 1.0 L min^{-1} H_2 and O_2, after equilibration at the following symmetric dew points: optimized (anode/cathode: 50 °C/50 °C), optimized +1 °C, the first 30 min at optimized +2 °C, and the performance "crashed condition" seen after 30 min at optimized +2 °C; (B) qualitative through-plane water distribution plots extracted from the data in A; (C) operando in-plane neutron radiographic images of a PFAEM-based AEMFC after equilibration at the following symmetric dew points: optimized (anode/cathode: 54 °C/51 °C), optimized +1 °C, optimized +2 °C, and a recovered cell at optimized dew points and 1.0 A cm^{-2} current density.

layer and gas diffusion layer (GDL), while the cathode catalyst layer and GDL show almost no RH dependence. At optimal +1 °C, liquid water accumulating in the anode catalyst layer and GDL was coupled with a 75 mV reduction in the cell voltage (Fig. S3, ESI†). As the dew points were increased to optimal +2 °C, liquid water accumulation further increased, and the cell voltage decreased an additional 50 mV (Fig. S3, ESI†). After 30 min at the optimal +2 °C condition, water further accumulated in the anode GDL, the severity of which was observed in the water distribution plot (Fig. 2B, pixels 0–10) and in the in the neutron image (right hand neutron image in Fig. 2A). This resulted in the cell losing its ability to support the 1.5 A cm^{-2} current density as the cell voltage fell to 0 V and the test stand could no longer operate galvanostatically at the set-point current (Fig. S3, ESI†). The cell performance observed, both steady-state and dynamic, gives insight into water management issues during AEMFC operation, notably: (i) the amount of water in the anode GDL increased significantly with inlet RH, eventually depriving the anode catalyst layer of sufficient reactant H_2 gas, highlighting the importance of anode water management; (ii) the total amount of water in the AEM was decreased after the flooding event, and a much lower water content was observed near the cathode interface than the anode interface as would be expected; and (iii) water in the cathode catalyst layer and the cathode GDL was independent of RH, even after 30 min at the optimal +2 °C condition where lower currents were observed.

The observed performance and water distribution profiles strongly suggest that back diffusion of water from the anode to the cathode is primarily responsible for keeping the AEM hydrated during cell operation, and is the critical source of water for the cathode reaction. Further, the back diffusion of water is primarily driven by the water production reaction within the anode, as when the cell stops producing water at the anode as the current drops (as in the case of optimal +2 °C @ 30 min), the water in the cathode catalyst layer and GDL remain largely unchanged even compared to the less humidified, optimal condition. These are new observations that have not been reported previously, though they are supported by the fact that low relative humidities at the cathode are needed to achieve the recent record AEM performance[20,34] since rapid liquid water transport coupled with high cathode gas dew points can lead to cathode flooding as well.[34] These observations also explain why high ionic conductivity and water transport rates are critical requirements in AEMFCs – water back diffusion is directly related to hydration and AEM ionic conductivity.[46] Low ionic conductivity in the AEM would not only yield high ohmic resistances (as expected), but would also lead to cathode dry-out due to the reduced level of water back diffusion; both of these effects not only limit the achievable current density, but also risk poor AEI stability and rapid chemical degradation of the AEMFC components.[6,42,47,48]

Identical neutron imaging experiments were performed with the same electrode design used in the radiation-grafted ETFE–BTMA AEM experiments, but replacing the membrane with a perfluorinated AEM (PFAEM, hydrated thickness = 45 μm).[21] These two membranes have very different chemical and physical properties despite their similar ionic conductivities (ETFE–BTMA: 132 mS cm^{-1}, PFAEM: 122 mS cm^{-1} at 80 °C, 95% relative humidity)[12,21] and functional headgroup. The PFAEM membrane has a lower ion-exchange capacity (IEC) than the radiation-grafted ETFE–BTMA membrane (0.91 meq g^{-1} *vs.* 2.01 meq g^{-1}) and lower water uptake (13 wt% *vs.* 53 wt%).[19,21] The AEMFCs constructed with the PFAEM required slightly higher optimal dew points in the gas feed streams (anode: 54 °C = 75%RH; cathode: 51 °C = 65%RH), possibly due to its lower water content, which can clearly be seen in Fig. 2C when compared to Fig. 2A. Despite the differences between these AEMs, very similar water content trends were observed in the AEMFCs, which indicates that the lessons learned regarding the AEM hydration and the availability of reactant water in the cathode are more generally applicable to AEMFCs, and not just a membrane-specific observation. One additional insight gained from the PFAEM AEMFC experiments was that following optimal +2 °C anode flooding, excess water could be relieved at the cathode by lowering the current density from 1.5 A cm^{-2} to 1.0 A cm^{-2} (Fig. S4, ESI†), demonstrating that water accumulation is dynamically controllable and reversible through a combination of the operating parameters. From the results above, it is clear that AEMFC performance is a balance between maintaining adequate AEM hydration and avoiding electrode flooding, and that AEMFCs are much more sensitive to water management than PEMFCs.

Returning to the fuel cell performances reported in Fig. 1, the slight inflection in the polarization curve of IC and the close position of the peak power current relative to the mass transport limiting current suggests that anode flooding was a concern. To investigate this, AEMFCs were assembled with an identical AEI : C : Pt weight ratio to IC (0.625 : 1.5 : 1), but with only 60% of the total anode catalyst layer loading, and hence a reduced catalyst layer thickness (denoted as r-IC). The undesirable effect of reducing the catalyst layer thickness was that the transition to mass transport control occurred at a much lower current density. This can be observed both by directly comparing the IC and r-IC polarization curves (Fig. 1 and Table 2) as well as taking a deeper look into intrinsic behavior by deconvoluting the polarization curves into their mass transport (Fig. 3A), ohmic (Fig. 3B) and kinetic (Fig. 3C and D) constituents, using a method first published by Gasteiger *et al.*[49]

Table 2 Electrochemical diagnostics and descriptions of the IC anode and the reduced loading anodes (r-IC and r-DC), including ECSA, currents at low overpotentials, peak power, and electrochemical impedance spectroscopy-(EIS)-derived data (details in the ESI)

Anode type		IC	r-IC	r-DC
ECSA	$m^2\ g^{-1}$	51.5	46.5	48.3
Anode loading – PtRu	mA cm^{-2}	0.72	0.42	0.42
Cathode loading – Pt	mA cm^{-2}	0.54	0.54	0.53
Current@0.90 V	mA cm^{-2}	51.9	49.9	48.1
Current@0.85 V	mA cm^{-2}	222	154	157
Current@0.80 V	mA cm^{-2}	612	321	347
Max power density	mW cm^{-2}	1690	783	904
OH^- transfer resistance	mΩ cm^2	49.4	54.7	47.0

As an additional diagnostic, the electrochemically active surface area (ECSA) was measured using the CO stripping technique. A representative *in situ* CO stripping voltammogram for a IC anode (ETFE–BTMA AEM) is shown in Fig. 3E, and the quantitative results for the ECSAs of both IC and r-IC are given in Table 2. The measured ECSAs (normalized by mass) of the two electrodes are very similar, showing that catalyst utilization is essentially identical. At first glance, the kinetic portion of the deconvoluted polarization data in Fig. 3C seem to show kinetic effects that influence performance. However, normalizing the kinetic overpotential by the catalyst mass (Fig. 3D) leads to a near-perfect overlay of the IC and r-IC curves, showing that these differences are largely explained by loading and that the kinetic behavior of the catalysts in these AEMFCs are essentially identical. This is also supported by comparing the current density at 0.9 V, an overpotential predominantly under kinetic control, where the magnitude of the kinetic current for the two cases are separated by a mere 2 mA cm^{-2}. The combination of the polarization and neutron imaging data shows that accumulation of anode water limits the performance of state-of-the-art AEMFCs, and that lower water capacity electrodes tended to have lower limiting currents.

Therefore, we sought to increase the water capacity of the anode while maintaining cell hydration through further manipulation of the AEI : C : Pt ratio in the anode catalyst layer. Electrodes were fabricated with the same catalyst loading as r-IC while doubling the loadings of both the carbon and the AEI (denoted as r-DC for double carbon). The result was that compared to r-IC, r-DC anodes saw an increase in the achievable current density of 35% (from 1.94 A cm^{-2} to 2.64 A cm^{-2}) and peak power of 15% (783 mW cm^{-2} to 904 mW cm^{-2}). Interestingly, from Fig. 3A up to a current density of *ca.* 1.2 A cm^{-2}, the mass transport overpotential for r-DC and r-IC overlay; a separation was only observed at higher current densities. Since the ECSA (catalyst utilization) for these two anodes are essentially identical, this separation is best explained by the pore volume inside the catalyst layer. Thus, (i) the C : Pt mass ratio is important because it sets a certain "thickness" for the removal/retention of water; and (ii) the AEI : C ratio is important as it effects the ionic conductivity (Table 2) and mobility of reactant water in the catalyst layer. In the case of high current operation, the excess water must be removed (to the cathode through the AEM as well as through the GDL into the anode exhaust), but under low current operation the water must be retained to avoid AEM dryout. Therefore, thinning of the catalyst layer is not advised, although this can create additional challenges when targeting low loaded electrodes. These findings, widely applicable to the AEMFC community, will immediately help researchers and companies in the field to design improved cells and systems.

However, it is certainly possible to add too much additional volume to the anode catalyst layer. One such case study is shown in Fig. S5 in the ESI,† that shows that kinetic losses due to the wide distribution of catalyst away from the AEM can become larger than the mass transport gains realized with the added porosity. Therefore, an optimal C-content exists yielding high catalyst activity but with maximized ionic transport and

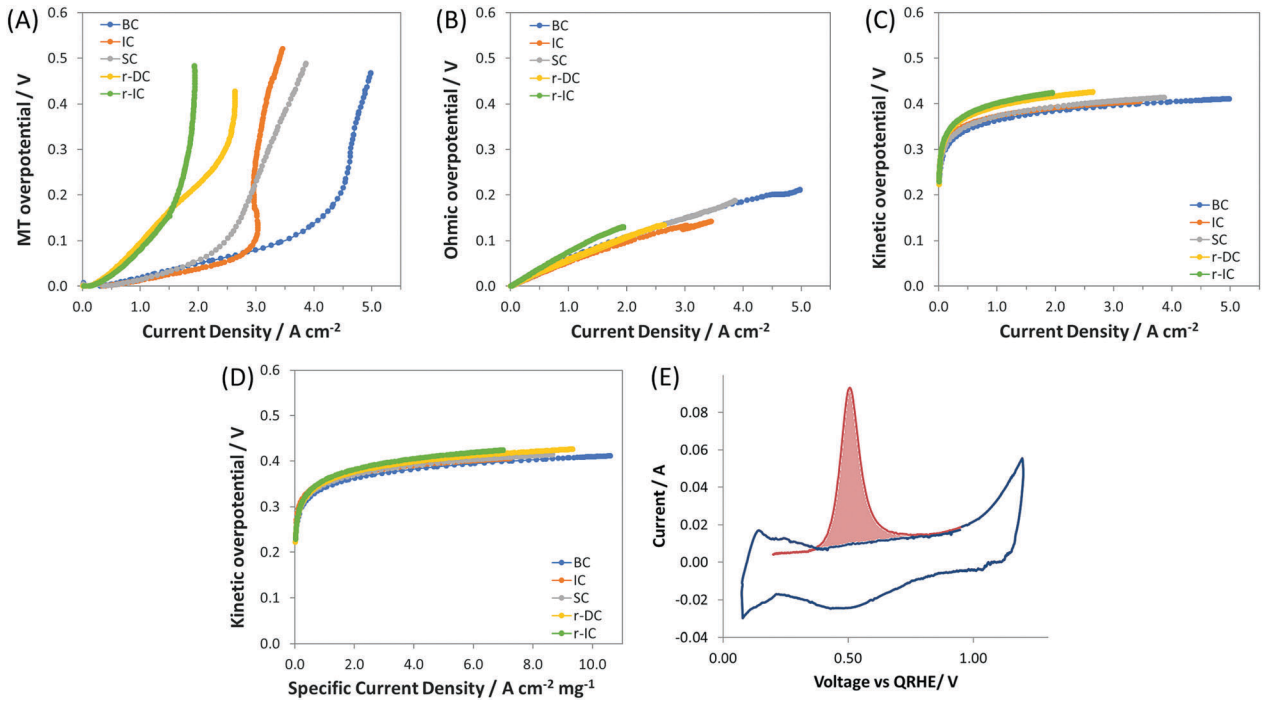

Fig. 3 Panels A–C show the overpotentials of ETFE–BTMA containing AEMFCs using near identical cathodes and different anodes (details given in Table 1), deconvoluted from the data in Fig. 1 into their: (A) mass transfer (MT), (B) ohmic, and (C) kinetic contributions; panel D shows plots of kinetic overpotential *vs.* mass corrected current density (Pt anode); panel E presents a representative CO stripping cyclic voltammogram used to determine the anode catalyst layer ECSA. First scan shown in red (with CO adsorbed); second scan (with CO removed) shown in blue.

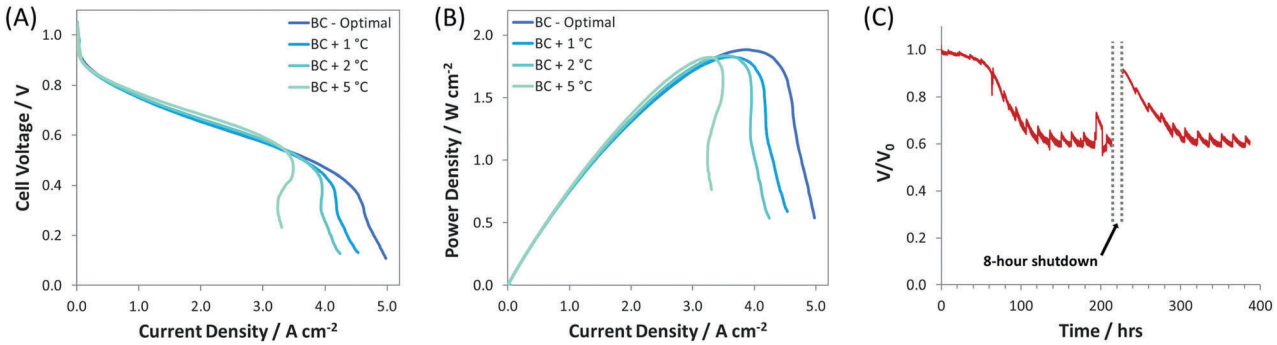

Fig. 4 (A) *i*–*V* and (B) *i*–power curves (10 mV s^{-1} forward scans) at increasing gas feed dew points for AEMFCs fabricated with the BC anode (details given in Table 1). The anode/cathode dew points for each test were: BC-optimal (45 °C/46 °C), BC + 1 °C (46 °C/47 °C), BC + 2 °C (47 °C/48 °C), BC + 5 °C (50 °C/50 °C); (C) 400 h AEMFC stability test at 600 mA cm^{-2} (with an 8 h cold shut down). The optimized anode/cathode dew points for the stability test were 52 °C/52 °C. For all experiments, the ETFE–BTMA membrane and AEI were used; the cell temperature was fixed at 60 °C; H_2 and O_2 were fed at flow rates of 1.0 L min^{-1} to the anode and cathode, respectively.

gas phase accessibility. To find this optimum, the amounts of carbon and AEI in the catalyst layer were reduced slightly relative to r-DC while maintaining the AEI : C ratio and the catalyst loading was returned to the same levels as SC and IC. This case (denoted as BC for balanced ionomer and carbon), had an optimized AEI : C : Pt ratio close to 1.0 : 2.5 : 1.0 (actual measured value was 0.94 : 2.5 : 1.0) and was thicker (compared to the SC, IC, r-IC, and r-DC) to facilitate increased water capacity/tolerance. These optimizations resulted in new AEMFC records for achievable mass transport limiting current (5 A cm^{-2}), current density at peak power (4 A cm^{-2}), and peak power density (1.9 W cm^{-2}), which are shown in Fig. 1. Importantly, this high-performance BC anode design is significantly less sensitive to changes in the gas feed dew points than the earlier configurations. Now, a 2 °C bilateral increase only results in a minimal 50 mW cm^{-2} reduction in peak power (Fig. 4) – not catastrophic flooding – and a 5 °C increase in the anode dew point only sacrifices 75 mW cm^{-2}. This is a significant and important improvement for the water tolerance and steady operation of AEMFCs. As a result, AEMFCs fabricated with a balanced AEI : C : Pt ratio at the anode were able to operate for >400 h (Fig. 4C). During this time, the cell retained 60% of its operating voltage (with only minor voltage decay over the last 300 h), with a recovery of performance after a simulated 8 hour cold shutdown where the reacting gases were removed and the cell was allowed to cool to room temperature.

These gains were exclusively made by understanding and improving the water mass transport characteristics of the operating AEMFC. The findings reported above have led to an AEMFC anode design that is so efficient, from a water management perspective, that mass transport is no longer the dominating loss in the cell; it is the ohmic resistance that is now limiting the cell performance (Fig. 3A and B). Therefore, with the very high ionic conductivity of the AEM and high activity of the catalysts, the results with the BC anode are likely approaching the maximum that is possible with AEMFCs (without the development of much thinner, robust AEMs that exhibit enhanced water back diffusion characteristics). The results of this also work show that AEMFCs can be performance-competitive with PEMFCs and have a promising future; expedited research is required working towards increased performance stability, application of non-PGM catalysts, lower-cost supporting components, and stack design and scaleup.

Author contributions

TJO was chiefly responsible for cell assembly and testing of the AEMFCs. XP, YZ, AMP and WEM also contributed to cell assembly and testing. TJO and AMP performed the ECSA measurements. LW synthesized the ETFE AEM. JRV oversaw the conception and synthesis of the ETFE–BTMA AEM and AEI. BSP oversaw the conception and synthesis of the PFAEM. WEM oversaw the conception, assembly and testing of all of the AEMFC electrodes and cells. DSH and JML oversaw the conception and execution of the NIST neutron imaging experiments, with JML also leading the cell assembly at NIST and DLJ leading the development of the data analysis tools. TJO and WEM were the primary authors of the manuscript and chiefly responsible for the data analysis, with JRV, BSP and DSH also contributing to the writing and analysis in minority roles.

Conflicts of interest

There are no conflicts of interest to declare.

Acknowledgements

The authors gratefully acknowledge the financial support of the US DOE Early Career Program Award Number DE-SC0010531 for the effort expended by T. J. O., X. P., and W. E. M. to perform this work as well as equipment and supplies. Y. Z. acknowledges assistance from the "Graduate Student International Cultivation of Zhejiang University" program. The PFAEM materials development and diagnostic techniques and equipment at the National Renewable Energy Laboratory was supported by the U.S. Department of Energy under Contract No. DE-AC36-08GO28308. NIST authors acknowledge assistance from Mr E. Baltic in the conduct

of the imaging measurements and funding from the Department of Energy interagency agreement No. DE_AI01-01EE50660. The ETFE-based materials used were developed and produced at the University of Surrey with financial support from The UK's Engineering and Physical Sciences Research Council (EPSRC grant EP/M014371/1).

References

1 Web of Science, Citation Report for 'Anion Exchange Membrane Fuel Cell' search, http://www.webofknowledge.com, accessed 19 December, 2017.
2 B. S. Pivovar, Alkaline Membrane Fuel Cell Workshop Final Report, Phoenix, AZ, 2016.
3 B. P. Setzler, Z. Zhuang, J. A. Wittkopf and Y. Yan, *Nat. Nanotechnol.*, 2016, **11**, 1020–1025.
4 A. Serov, I. V. Zenyuk, C. G. Arges and M. Chatenet, *J. Power Sources*, 2018, **375**, 149–157.
5 S. Gottesfeld, D. R. Dekel, M. Page, C. Bae, Y. Yan, P. Zelenay and Y. S. Kim, *J. Power Sources*, 2018, **375**, 170–184.
6 D. R. Dekel, *J. Power Sources*, 2018, **375**, 158–169.
7 C. H. Park, S. Y. Lee, D. S. Hwang, D. W. Shin, D. H. Cho, K. H. Lee, T. W. Kim, T. W. Kim, M. Lee, D. S. Kim, C. M. Doherty, A. W. Thornton, A. J. Hill, M. D. Guiver and Y. M. Lee, *Nature*, 2016, **532**, 480–483.
8 J. R. Varcoe, P. Atanassov, D. R. Dekel, A. M. Herring, M. A. Hickner, P. A. Kohl, A. R. Kucernak, W. E. Mustain, K. Nijmeijer, K. Scott, T. Xu and L. Zhuang, *Energy Environ. Sci.*, 2014, **7**, 3135–3191.
9 J. Ponce-González, D. K. Whelligan, L. Wang, R. Bance-Soualhi, Y. Wang, Y. Peng, H. Peng, D. C. Apperley, H. N. Sarode, T. P. Pandey, A. G. Divekar, S. Seifert, A. M. Herring, L. Zhuang and J. R. Varcoe, *Energy Environ. Sci.*, 2016, **9**, 3724–3735.
10 T. P. Pandey, H. N. Sarode, Y. Yang, Y. Yang, K. Vezzù, V. Di Noto, S. Seifert, D. M. Knauss, M. W. Liberatore and A. M. Herring, *J. Electrochem. Soc.*, 2016, **163**, H513–H520.
11 L. A. Adams, S. D. Poynton, C. Tamain, R. C. T. Slade and J. R. Varcoe, *ChemSusChem*, 2008, **1**, 79–81.
12 T. P. Pandey, A. M. Maes, H. N. Sarode, B. D. Peters, S. Lavina, K. Vezzù, Y. Yang, S. D. Poynton, J. R. Varcoe, S. Seifert, M. W. Liberatore, V. Di Noto and A. M. Herring, *Phys. Chem. Chem. Phys.*, 2015, **17**, 4367–4378.
13 M. Mamlouk, J. A. Horsfall, C. Williams and K. Scott, *Int. J. Hydrogen Energy*, 2012, **37**, 11912–11920.
14 R. Espiritu, M. Mamlouk and K. Scott, *Int. J. Hydrogen Energy*, 2016, **41**, 1120–1133.
15 J. Pan, C. Chen, Y. Li, L. Wang, L. Tan, G. Li, X. Tang, L. Xiao, J. Lu and L. Zhuang, *Energy Environ. Sci.*, 2014, **7**, 354–360.
16 L. Zhu, J. Pan, Y. Wang, J. Han, L. Zhuang and M. A. Hickner, *Macromolecules*, 2016, **49**, 815–824.
17 J. Xu, P. Gao and T. S. Zhao, *Energy Environ. Sci.*, 2012, **5**, 5333–5339.
18 X. Luo, A. Wright, T. Weissbach and S. Holdcroft, *J. Power Sources*, 2018, **375**, 442–451.
19 L. Q. Wang, E. Magliocca, E. L. Cunningham, W. E. Mustain, S. D. Poynton, R. Escudero-Cid, M. M. Nasef, J. Ponce-González, R. Bance-Souahli, R. C. T. Slade, D. K. Whelligan and J. R. Varcoe, *Green Chem.*, 2017, **19**, 831–843.
20 L. Wang, J. J. Brink, Y. Liu, A. M. Herring, J. Ponce-González, D. K. Whelligan and J. R. Varcoe, *Energy Environ. Sci.*, 2017, 2154–2167.
21 A. M. Park, Z. R. Owczarczyk, L. E. Garner, A. C. Yang-Neyerlin, H. Long, C. M. Antunes, M. R. Sturgeon, M. J. Lindell, S. J. Hamrock, M. Yandrasits and B. S. Pivovar, *ECS Trans.*, 2017, **80**, 957–966.
22 Y. Wang, G. Wang, G. Li, B. Huang, J. Pan, Q. Liu, J. Han, L. Xiao, J. Lu and L. Zhuang, *Energy Environ. Sci.*, 2015, **8**, 177–181.
23 J. Durst, A. Siebel, C. Simon, F. Hasché, J. Herranz and H. A. Gasteiger, *Energy Environ. Sci.*, 2014, **7**, 2255–2260.
24 W. Sheng, Z. Zhuang, M. Gao, J. Zheng, J. G. Chen and Y. Yan, *Nat. Commun.*, 2015, **6**, 1–6.
25 W. Sheng, M. Myint, J. G. Chen and Y. Yan, *Energy Environ. Sci.*, 2013, **6**, 1509.
26 X. Peng, T. J. Omasta, J. M. Roller and W. E. Mustain, *Front. Energy*, 2017, **14**, 299–309.
27 M. Alesker, M. Page, M. Shviro, Y. Paska, G. Gershinsky, D. R. Dekel and D. Zitoun, *J. Power Sources*, 2016, **304**, 332–339.
28 S. A. Kabir, K. Lemire, K. Artyushkova, A. Roy, M. Odgaard, D. Schlueter, A. Oshchepkov, A. Bonnefont, E. Savinova, D. Sabarirajan, P. Mandal, E. Crumlin, I. V. Zenyuk, P. Atanassov and A. Serov, *J. Mater. Chem. A*, 2017, **5**, 24433–24443.
29 H. A. Miller, F. Vizza, M. Marelli, A. Zadick, L. Dubau, M. Chatenet, S. Geiger, S. Cherevko, H. Doan, R. K. Pavlicek, S. Mukerjee and D. R. Dekel, *Nano Energy*, 2017, **33**, 293–305.
30 H. A. Miller, A. Lavacchi, F. Vizza, M. Marelli, F. Di Benedetto, F. D'Acapito, Y. Paska, M. Page and D. R. Dekel, *Angew. Chem., Int. Ed.*, 2016, **55**, 6004–6007.
31 Z. Zhuang, S. A. Giles, J. Zheng, G. R. Jenness, S. Caratzoulas, D. G. Vlachos and Y. Yan, *Nat. Commun.*, 2016, **7**, 1–8.
32 R. Gokhale, Y. Chen, A. Serov, K. Artyushkova and P. Atanassov, *Electrochem. Commun.*, 2016, **72**, 140–143.
33 L. Wang, J. J. Brink and J. R. Varcoe, *Chem. Commun.*, 2017, **53**, 11771–11773.
34 T. J. Omasta, L. Wang, X. Peng, C. A. Lewis, J. R. Varcoe and W. E. Mustain, *J. Power Sources*, 2018, **375**, 205–213.
35 Anion-Exchange Membranes for Energy Generation Technologies Workshop, Guildford, UK, 2013.
36 7th Bishop's Lodge Workshop: Materials for Energy Conversion Workshop, Santa Fe, NM, 2013.
37 Beijing Forum on Electrochemical Frontier Alkaline Membrane Fuel Cells: Catalysis & Materials, Wuhan, China, 2016.
38 Workshop on Ion Exchange Membranes for Energy Applications, Bad Zwischenahn, Germany, 2017.
39 S. D. Poynton, R. C. T. Slade, T. J. Omasta, W. E. Mustain, R. Escudero-Cid, P. Ocón and J. R. Varcoe, *J. Mater. Chem. A*, 2014, **2**, 5124–5130.

40 R. B. Kaspar, M. P. Letterio, J. A. Wittkopf, K. Gong, S. Gu and Y. Yan, *J. Electrochem. Soc.*, 2015, **162**, F483–F488.
41 D. R. Dekel, S. Willdorf, U. Ash, M. Amar, S. Pusara, S. Dhara, S. Srebnik and C. E. Diesendruck, *J. Power Sources*, 2018, **375**, 351–360.
42 D. R. Dekel, I. G. Rasin, M. Page and S. Brandon, *J. Power Sources*, 2018, **375**, 191–204.
43 H.-S. Shiau, I. V. Zenyuk and A. Z. Weber, *J. Electrochem. Soc.*, 2017, **164**, E3583–E3591.
44 D. S. Hussey, D. L. Jacobson, M. Arif, K. J. Coakley and D. F. Vecchia, *J. Fuel Cell Sci. Technol.*, 2010, **7**, 21024.
45 J. S. Preston, U. Pasaogullari, D. S. Hussey and D. L. Jacobson, *ECS Trans.*, 2011, **41**, 319–328.
46 T. D. Myles, A. M. Kiss, K. N. Grew, A. A. Peracchio, G. J. Nelson and W. K. S. Chiu, *J. Electrochem. Soc.*, 2011, **158**, B790.
47 L. Liu, X. Chu, J. Liao, Y. Huang, Y. Li, Z. Ge, M. A. Hickner and N. Li, *Energy Environ. Sci.*, DOI: 10.1039/C7EE02468A.
48 D. W. Shin, M. D. Guiver and Y. M. Lee, *Chem. Rev.*, 2017, **117**, 4759–4805.
49 H. A. Gasteiger, J. E. Panels and S. G. Yan, *J. Power Sources*, 2004, **127**, 162–171.